A short synthesis of delavatine A unveils new insights into site-selective cross-coupling of 3,5-dibromo-2-pyrone

Vignesh Palani,[†] Cedric L. Hugelshofer,[†] Ilia Kevlishvili,[§] Peng Liu,*[,§] and Richmond Sarpong*[,†]

[†] Department of Chemistry, University of California, Berkeley, CA 94720 (USA)

[§] Department of Chemistry, University of Pittsburgh, Pittsburgh, PA 15260 (USA)

Supporting Information Placeholder

ABSTRACT: The recognition of latent symmetry in delavatine A has enabled a short synthesis of the natural product starting from 3,5-dibromo-2-pyrone. The concise synthetic route features a cascade process involving a 6π electrocyclization to construct the indane core of delavatine A. In addition, we have conducted detailed experimental and computational studies to gain in-depth understanding of the mechanism of the observed site-selective cross-coupling of 3,5-dibromo-2-pyrone. This insight may provide new avenues to achieve the selective cross-coupling of multiply-halogenated heteroarenes.

Introduction

Plants of the *Incarvillea* genus, native to the Himalayas and Southwest China, have attracted considerable interest because of their use in traditional herbal medicine.[1] *Incarvillea delavayi* has been used as a medicinal plant to treat anemia, rheumatism and dizziness.[2] Recently, a structurally unique alkaloid, delavatine A (**1**, Scheme 1a) was isolated from *I. delavayi* by Zhang and co-workers. This unusual isoquinoline-containing alkaloid displays micromolar antitumor activity against a number of human cancer cell lines.[3] Not surprisingly, the unique architecture and novel biological activity of **1** has made it an attractive synthetic target. An elegant total synthesis of **1** was recently reported by Li et al. that featured an asymmetric hydrogenation of an indenyl olefin group as well as the application of a triflamide-directed C–H olefination method (Scheme 1a).[4a]

Biosynthetically, it has been proposed that delavatine A (**1**) is derived from trisaldehyde **4** (Scheme 1b).[3] On this basis, our synthetic design targeted a final stage, bioinspired, condensation of **4** with an ammonia source to yield the isoquinoline moiety in **1**. Furthermore, we recognized the latent symmetry in **4** (see highlighted cyclopentenyls), which we envisioned could translate into an elegant and powerful retrosynthetic disconnection. Leveraging molecular symmetry (both hidden and overt) in total synthesis is especially powerful as it may facilitate the identification of radically simplified precursors, and in this way enhance synthetic efficiency.[5]

By taking advantage of the latent symmetry of **4**, we also sought to devise a modular and convergent synthetic route to **4** through an ambitious cascade sequence starting from pseudosymmetric pyrone **7**. More specifically, it was anticipated that the indane core of **4** would be forged by 6π electrocyclization[6] of cross-conjugated dienolate **5**, which in turn would arise from the highly conjugated polyene **6**. Given the inherent pseudosymmetry of pyrone **7**, this intermediate was traced

Scheme 1. Retrosynthetic plan and site-selective cross-coupling of 3,5-dibromo-2-pyrone

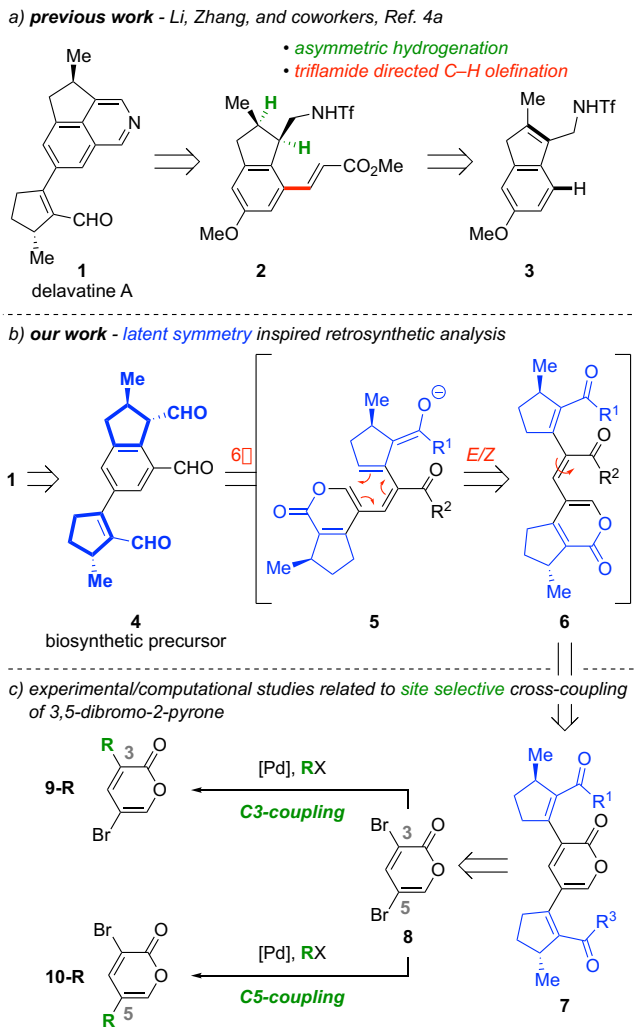

back to known 3,5-dibromo-2-pyrone (**8**)[7] and the corresponding cyclopentenyl coupling partners (highlighted in blue in pyrone **7**) through site-selective cross-coupling reactions.

3,5-Dibromo-2-pyrone (**8**) is an α-pyrone derived polyhalogenated heterocycle bearing two chemically inequivalent C–Br bonds.[8] Site-selective modifications of **8**, leading to constitutional isomeric products, have been demonstrated by Cho and co-workers in various cross-coupling processes.[9–11] While certain experimental conditions have been established that enable site-selective coupling in **8**, the mechanistic rationale for this observed selectivity has not been unequivocally established. Site-selective cross-coupling reactions of polyhalogenated heterocycles[12] allow highly efficient retrosynthetic disconnections and have evolved to be invaluable transformations for both academic and industrial researchers.[13] While several studies aimed at understanding the basis of site-selective couplings have emerged over the past decade,[14] predicting and rationalizing the selectivity outcome has oftentimes remained challenging.[8,12a] In some polyhaloaromatic compounds, consideration of ^{1}H NMR chemical shifts of the C–H bonds in the corresponding non-halogenated aromatic compounds can guide the prediction of site-selective transformations.[15] However, the cross-coupling of 3,5-dibromo-2-pyrone (**8**) gives rise to products that are contrary to this predicted outcome.[8] Hence, we sought to gather further mechanistic insight to guide predictable, site-selective couplings in **8**.

Mechanistic Studies

On the basis of previous studies conducted by Cho and co-workers, we recognized that solvent choice, temperature, and addition of copper iodide appeared to have a marked influence on the observed coupling selectivity in **8**.[9–11] Table 1 summarizes our results of the site-selective Suzuki coupling of **8** and phenyl boronic acid. Consistent with the results of Cho et al.,[10] we found that in non-polar solvents, such as 1,2-dichloroethane, tetrahydrofuran, and toluene, C3-coupled product **9** was primarily formed. In these solvents, neither the addition of CuI nor conducting the reaction at elevated temperature affected the observed site-selectivity. Interestingly, in more polar solvents, such as dimethyl sulfoxide, dimethylformamide, and acetone, C5-coupled product **10** was generally formed as the major product. However, **9** was formed in the absence of CuI and when the reaction was conducted in acetone.[16] In contrast to the observations of Cho et al.,[11] we did not observe a switch in the site-selectivity upon increasing the reaction temperature from 23 °C to 50 °C. Overall, we found the selectivity of the cross-coupling reactions to be non-temperature dependent, and to proceed predominantly at the C3-position in non-polar solvents, while coupling is favored at the C5 position in polar solvents in the presence of CuI.

To gain more insight into the effect of CuI in these cross-coupling reactions, we chose to revisit several oxidative addition experiments previously conducted by Cho and co-workers,[10,11] and analyze the relative stabilities of the resulting C3 and C5-Pd complexes (**12** and **13**, Table 2).[17] We observed that when the oxidative addition was conducted in non-polar solvents (toluene) only C3-Pd complex **12** was formed, irrespective of the reaction temperature or whether CuI was added.

Table 1. Suzuki couplings with 3,5-dibromo-2-pyrone

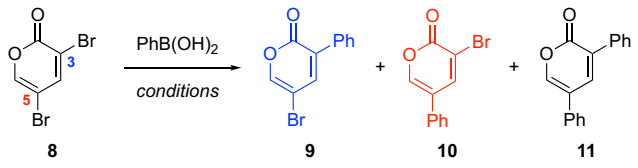

	ε[a]	Solvent	yield[b] (%) **9:10:11** Δ (w/o CuI)	rt (w/ CuI)	Δ (w/ CuI)
increasing polarity ↑	47	DMSO	—[c]	nd:12:nd	8:13:nd
	38.25	DMF	tr:nd:nd	nd:18:nd	15:37:nd
	21.01	acetone	53:nd:nd	tr:32:nd	16:29:nd
	10.42	DCE	70:nd:nd	57:13:nd	58:tr:11
	7.52	THF	47:nd:19	27:8:nd	49:17:nd
	2.38	toluene	52:nd:nd	55:tr:nd	56:tr:tr

[a]Dielectric constant at 20 °C.[18] [b]Determined by ^{1}H NMR analysis using 1,1,2,2-tetrachloroethane as an internal standard. [c]Decomposition of **8**. Conditions: $PhB(OH)_2$ (1.2 equiv), $Pd(PPh_3)_4$ (10 mol%), CuI (1.0 equiv), K_2CO_3 (2.0 equiv), solvent (0.1 M). nd = not detectable, tr = trace.

In polar solvents (DMF), we observed the formation of **12** when the reaction was conducted in the absence of CuI, while C5-Pd complex **13** was formed as the major product in the presence of CuI. The structures of **12** and **13** were unambiguously confirmed by single-crystal X-ray analysis.[19] Notably, these oxidative addition experiments are also supported by the observed position selectivity in Suzuki coupling of **8** (Table 1), where the C5-coupled product (**10**) was only formed in polar solvents and in the presence of CuI.

Table 2. Oxidative addition experiments

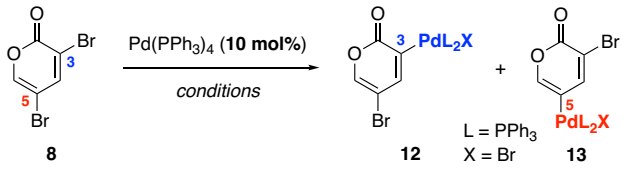

Solvent	yield[a] (%) **12:13** rt (w/o CuI)	Δ (w/o CuI)	rt (w/ CuI)	Δ (w/ CuI)
DMF	31:nd	39:nd	11:20	14:23
toluene	32:nd	50:nd	29:nd	50:nd

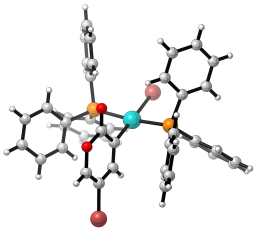

12-trans [X-ray]

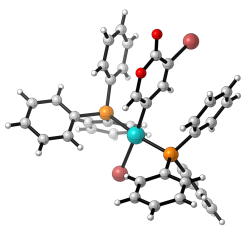

13-trans [X-ray]

[a]Determined by ^{1}H NMR analysis using 1,1,2,2-tetrachloroethane as an internal standard. The NMR yields were calculated with respect to the amount of $Pd(PPh_3)_4$ used (10 mol%). Conditions: $Pd(PPh_3)_4$ (10 mol%), CuI (1.0 equiv), solvent (0.1 M). nd = not detectable.

Next, the oxidative addition experiments were carried out at different reaction temperatures in the presence of CuI with

DMF as the solvent (Figure 1). It was observed that C5 Pd oxidative adduct **13** was favored at lower temperatures whereas at elevated temperature, C3 Pd oxidative adduct **12** was formed as the major product. Further experiments revealed that C5 Pd oxidative adduct **13** converts to C3 Pd oxidative adduct **12** in DMF in the presence of CuI at elevated temperatures and over prolonged reaction periods.[20]

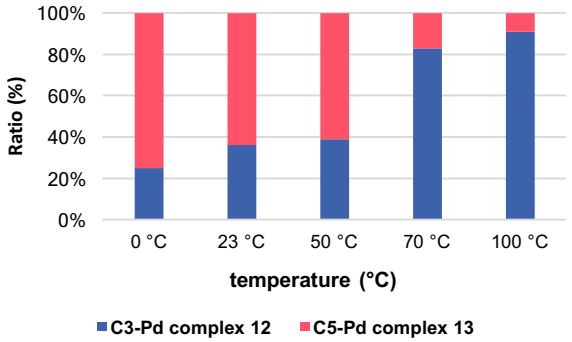

Figure 1. Influence of temperature on ratios of C3- to C5-Pd complexes. Conditions: $Pd(PPh_3)_4$ (10 mol%), CuI (1.0 equiv), DMF (0.1 M).

Interestingly, when a mixture of Pd oxidative adducts **12** and **13** was treated with tributylphenylstannane in DMF, only the C5-coupled product (**10**) was formed,[20] indicating that **12** can also interconvert to **13** prior to cross-coupling. In summary, our observations indicate that C5-Pd complex **13** is the *kinetic* oxidative adduct whereas C3-Pd complex **12** is the *thermodynamic* oxidative adduct. Moreover, **12** and **13** can interconvert, and the rate of transmetallation/reductive elimination is faster for C5-Pd complex **13** when compared to that of C3-Pd complex **12**. This describes a Curtin–Hammett scenario[21] wherein rapid interconversion of the Pd-complexes (**12** and **13**) occurs, and where the ratio of the resulting cross-coupled products (i.e., **9**:**10**) is solely dependent on the energy difference between the two respective rate-limiting transition states of transmetallation/reductive elimination.

Computational Insight

We sought to gain additional insight into the origins of the effects of CuI and solvent on the kinetic and thermodynamic selectivities of the oxidative addition through computational studies. Density functional theory (DFT) calculations were performed at the M06/6-311+G(d,p)–SDD/SMD(DMF)//B3LYP/6-31G(d)–SDD level of theory.[20] We first computationally considered the Lewis-acid activation of the pyrone through coordination of CuI or cationic $(DMF)Cu^+$ to the carbonyl group of **8**. However, these results indicated that the CuI or Cu^+ coordination has a minimal impact on the site-selectivity of oxidative addition,[20] and thus cannot explain the experimentally observed site-selectivity trend under the different conditions. Additionally, we considered the pathway involving oxidative addition of pyrone **8** to CuI[22] ($\Delta G^{\ddagger}$ = 27.2 kcal/mol, with respect to the pyrone-CuI π-complex). This pathway requires a higher barrier than the oxidative addition to Pd(0) and does not support the observed reversal of site-selectivity in the presence of CuI.[(20)] As such, we surmised that in the presence of CuI the oxidative addition may occur through an alternative mechanism with a different active Pd catalyst. Because previous computational studies have suggested a bis-phosphine ligated Pd complex is more favored for oxidative addition with PPh_3 as ligand,[23] the oxidative addition in the absence of CuI is expected to occur via tri-coordinated $(PPh_3)_2Pd(0)$-pyrone complex **14** (Scheme 2). Additionally, on the basis of empirically established precedent supporting the ability of CuI to promote phosphine ligand exchange at Pd,[24] we hypothesized that CuI could have a similar effect in this system. In this way, CuI could promote phosphine ligand dissociation from **14** to form a mono-phosphine ligated Pd complex (**16** or **17**, Scheme 2) as the operative intermediate in the catalytic cycle, which has been reported to be relatively more reactive toward oxidative addition.[25] Indeed, our DFT calculations show that exchanging one of the PPh_3 ligands in **14** with $(DMF)_2CuI$ (**15**) to form mono-phosphine ligated Pd complexes **17** and **16** are both thermodynamically feasible,[26] indicating an equilibrium between the bis- and mono-phosphine ligated Pd complexes before the oxidative addition step. Furthermore, in the absence of CuI, formation of the mono-phosphine ligated Pd complexes is highly endergonic ($\Delta G \geq 13$ kcal/mol),[20] indicating the bis-phosphine ligated Pd complex **14** is operative under these conditions.

Scheme 2. Computed ligand exchange energies from the bis-phosphine ligated Pd complex 14 to form mono-phosphine ligated Pd complexes 16 and 17.

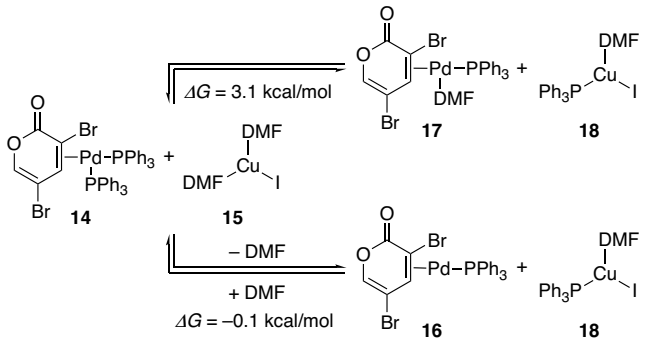

Therefore, we computed the oxidative addition pathways from complexes **14** (Figure 2A), **16** (Figure 2B), and **17** (Figure S3A in the Supporting Information). Interestingly, the oxidative additions of **14** and **16** have very different site-selectivity outcomes. In the bis-phosphine ligated Pd complex pathway, the barrier for the oxidative addition at C3 (**TS1**; Figure 2A) is 3.5 kcal/mol lower than that at C5 (**TS2**). Following *cis*/*trans* isomerization of the phosphine ligands on the oxidative addition complexes (*i.e.*, **12-cis** and **13-cis**, respectively), the C3 adduct (**12-trans**) is slightly (0.3 kcal/mol) more stable than the C5 adduct (**13-trans**). These results are consistent with the experimentally observed C3-selectivity for oxidative addition in DMF and toluene in the absence of CuI (see Table 2). To understand the factors governing the C3 site-selectivity, we performed a distortion/interaction analysis to investigate the distortion energies of the catalyst ($\Delta E_{dist\text{-}cat}$) and the pyrone substrate ($\Delta E_{dist\text{-}sub}$) to reach their transition state geometries as well as the stabilizing interaction energy (ΔE_{int}) between the two fragments (Figure 2A).[27] Although the C3-oxidative addition has an earlier transition state, as evidenced by the smaller substrate distortion energy ($\Delta E_{dist\text{-}sub}$) and the shorter C–Br bond distance in **TS1**, the interaction between the catalyst and the substrate in

TS1 (ΔE_{int}) is still stronger than that in **TS2** by 2.6 kcal/mol. The stronger catalyst-substrate interaction is due to a more favorable frontier molecular orbital (FMO) interaction between the LUMO(π^*) of **8** and the HOMO (d_{xy}) of the Pd in **TS1**.[14a] The computed LUMO of **8** showed a much larger coefficient at the C3-position than at the C5 position (Figure 2A inset).[28]

In the presence of CuI, the C3 and C5 oxidative additions of the mono-phosphine ligated Pd complex **16** (**TS3** and **TS4**, respectively, Figure 2B) both require lower barriers as compared to those of bis-phosphine ligated Pd complex **14**. Notably, the mono-phosphine ligated Pd complex oxidative addition no longer kinetically favors the formation of C3-Pd complex **12** and the barriers for **TS3** and **TS4** are comparable. This is consistent with the low selectivity for the site of oxidative addition observed empirically in the presence of CuI in DMF (Table 2). Distortion/interaction analysis of **TS3** and **TS4** reveals that **TS3** has a more favorable interaction energy as compared to **TS4**. However, **TS3** is a later transition state with greater distortion penalty of the substrate ($\Delta E_{dist\text{-}sub}$), which compensates for the interaction energy difference and leads to similar barriers for the two oxidative addition transition states. In this mono-phosphine ligated Pd complex pathway, Pd is less nucleophilic due to a lower-lying HOMO.[29] Therefore, the FMO interaction between the Pd center and the substrate is less prominent and the preference for the C3 oxidative addition selectivity is diminished.

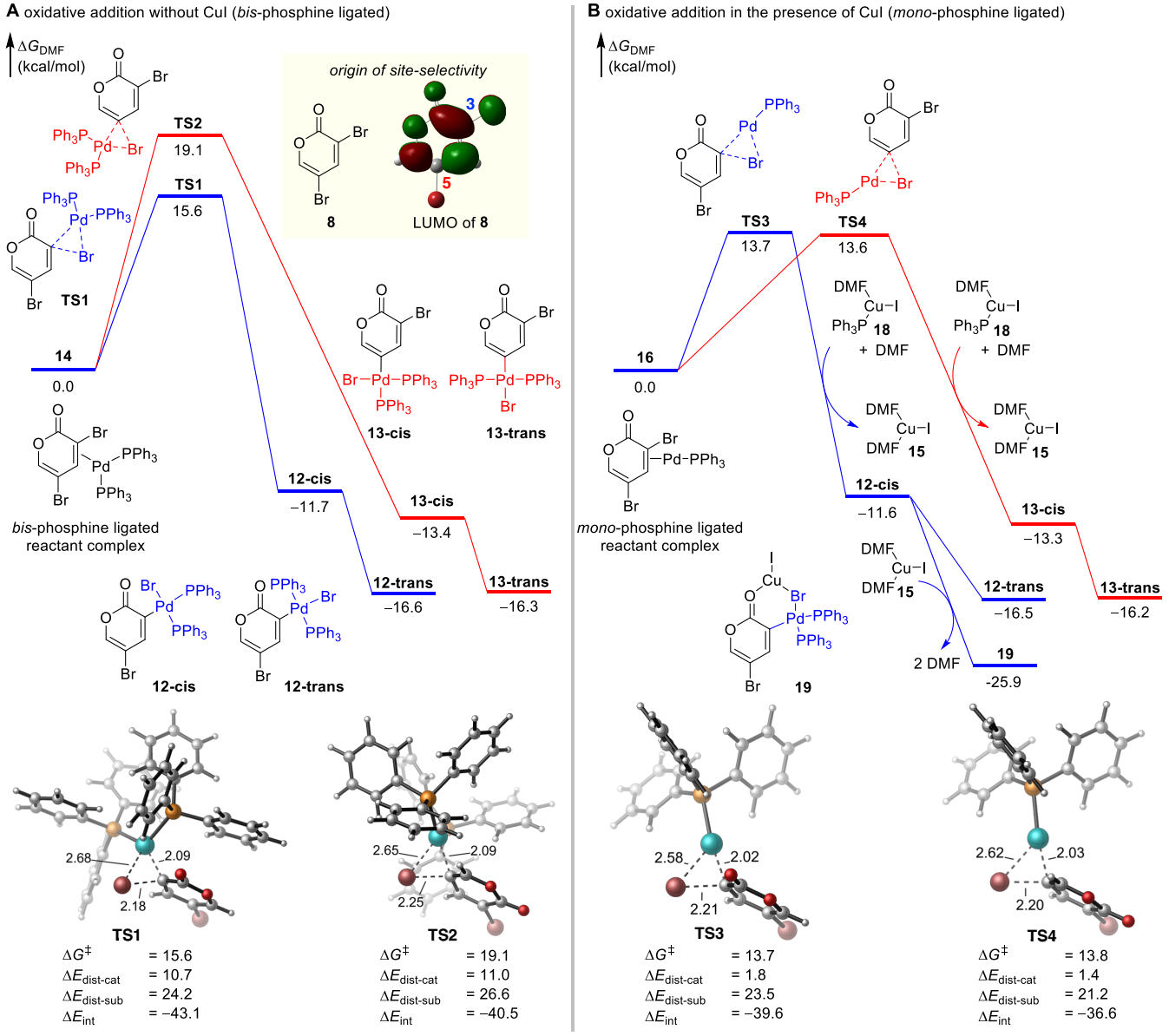

Figure 2. A) Oxidative addition of the bis-phosphine ligated Pd complex **14** at the C3- (shown in blue) and C5- (in red) positions of 3,5-dibromo-2-pyrone **8** in the absence of CuI. **B)** Oxidative addition of the mono-phosphine ligated Pd complex **16** in the presence of CuI. The distortion energies of the PdL_n catalyst ($\Delta E_{dist\text{-}cat}$) and the pyrone substrate ($\Delta E_{dist\text{-}sub}$), and the interaction energies between these two fragments in the oxidative addition transition states (ΔE_{int}) are provided. All energies in Figure 2A are with respect to **14**. All energies in Figure 2B are with respect to **16**, **18**, and DMF.

We also considered the oxidative additions of the DMF-coordinated mono-phosphine ligated Pd complex **17**. From **17**, the selectivity between the C3 and C5 oxidative addition transition states is also diminished ($\Delta\Delta G^{\ddagger}$ = 0.8 kcal/mol).[20] Overall, these results highlight a significant effect of the number of PPh_3 ligands on the selectivity of oxidative addition. While oxidative addition of bis-phosphine ligated Pd complex **14** is strongly preferred at C3, the site-selectivity is diminished in reactions with the mono-phosphine ligated Pd complexes (**16** or **17**).

Following oxidative addition, the more electron-deficient Pd(II) adduct binds another PPh_3 through ligand exchange with the CuI-phosphine complex to form tetracoordinated Pd(II) complexes **12** and **13** (Figure 2B). The *cis* isomer of the C3 adduct (**12-cis**) can bind to CuI to form a relatively stable ternary Cu complex (**19**) in which the Cu center is coordinated to both the pyrone carbonyl oxygen and the bromide attached to the Pd center. It should be noted that similar chelating complexes cannot be formed from **13-cis**, or either of the trans-isomers.[20] Because of the greater stability of **19** compared to other C3 and C5 adducts, the C3 oxidative addition pathway is thermodynamically more favorable.[(20)] This is consistent with the experimentally observed trend that increasing temperature leads to the C3 adduct as the major product (Figure 1).

With computational results in hand that explain the role of CuI in facilitating formation of a mono-phosphine ligated Pd complex (**16** or **17**) which in turn kinetically favors the formation of C5-Pd complex **13**, we sought experimental evidence to support this pathway. Toward this end, we analyzed the ratio of the generated C3 to C5-Pd complexes when the oxidative addition was carried out with varying concentrations of triphenylphosphine (Figure 3). Interestingly, we observed that when the concentration of triphenylphosphine was increased, C3-Pd complex **12** was predominantly formed. Hence, we postulated that higher concentrations of PPh_3 favor the oxidative addition pathway involving a bis-phosphine ligated Pd complex which leads to formation of C3-Pd complex **12**, in concert with our computational studies.

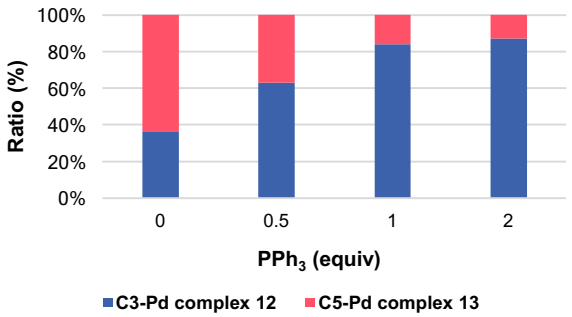

Figure 3. Effect of PPh_3 on the observed ratio of C3- to C5-Pd complex. Conditions: $Pd(PPh_3)_4$ (10 mol%), CuI (1.0 equiv), PPh_3, DMF (0.1 M), 23 °C.

Furthermore, we repeated the oxidative addition studies in the presence of other phosphine ligands.[20] We observed a preference for the formation of C5-Pd complex **13** when the oxidative addition was carried out using bulky phosphine ligands. This observation supports the rationale that the C5-Pd complex **13** is generated when the oxidative addition proceeds via a mono-phosphine ligated Pd complex, which is favored at lower PPh_3 concentrations or in the presence of bulkier phosphine ligands. The conclusions drawn from these experiments are in good agreement with our computationally-derived results.

We next sought to gain computational insight into the origin of C5-site-selectivity of the Stille coupling reactions under conditions where oxidative addition has been established to be reversible (see Table S6 for experimental details).[30] In these cases, the selectivity is expected to be determined in the subsequent transmetallation or reductive elimination steps. We calculated the C3- and C5-selective pathways for the transmetallation and reductive elimination steps from the oxidative adducts **12** and **13** using trimethylphenylstannane as a model coupling partner (Figure 4). We located the cyclic transmetallation transition states where the substrate and bromide are either cis- or trans- disposed. In accordance with previous computational studies,[31] the trans-transmetallation transition states (**TS5** and **TS6**) are about 5-6 kcal/mol more favorable than the corresponding cis-TS. The transition state associated with the transmetallation of the C5-adduct (**TS6**) is 2.0 kcal/mol more favorable than that of the C3-adduct (**TS5**) (Figure 4A).

These computational results are consistent with the empirically observed preferable coupling of **13** over **12**, when this mixture is exposed to tributylphenylstannane.[20] To better understand the origin of this preference, we considered the polarity of the transmetallation transition states. We hypothesized that since **TS6** is significantly more polar than **TS5** due to the greater separation of the partial positive (on Pd) and negative (on the pyrone carbonyl oxygen) charges, more favorable stabilization of this transition state would occur in a polar solvent. In support of this hypothesis, we calculated the gas phase energies for **TS5** and **TS6**. These calculations show that the relative stability is reversed in the gas phase, where **TS5** is favored by 2.6 kcal/mol (Figure 4B). Therefore, the polar solvent plays an important role in determining the selectivity for transmetallation. The transmetallation and subsequent ligand exchange with $CuI(PPh_3)(DMF)$ **18** leads to a four-coordinate Pd^{II} species (**20** or **21**), which then undergoes reductive elimination via either a bis-phosphine or mono-phosphine ligated transition state to form coupling products **9** and **10**.[20]

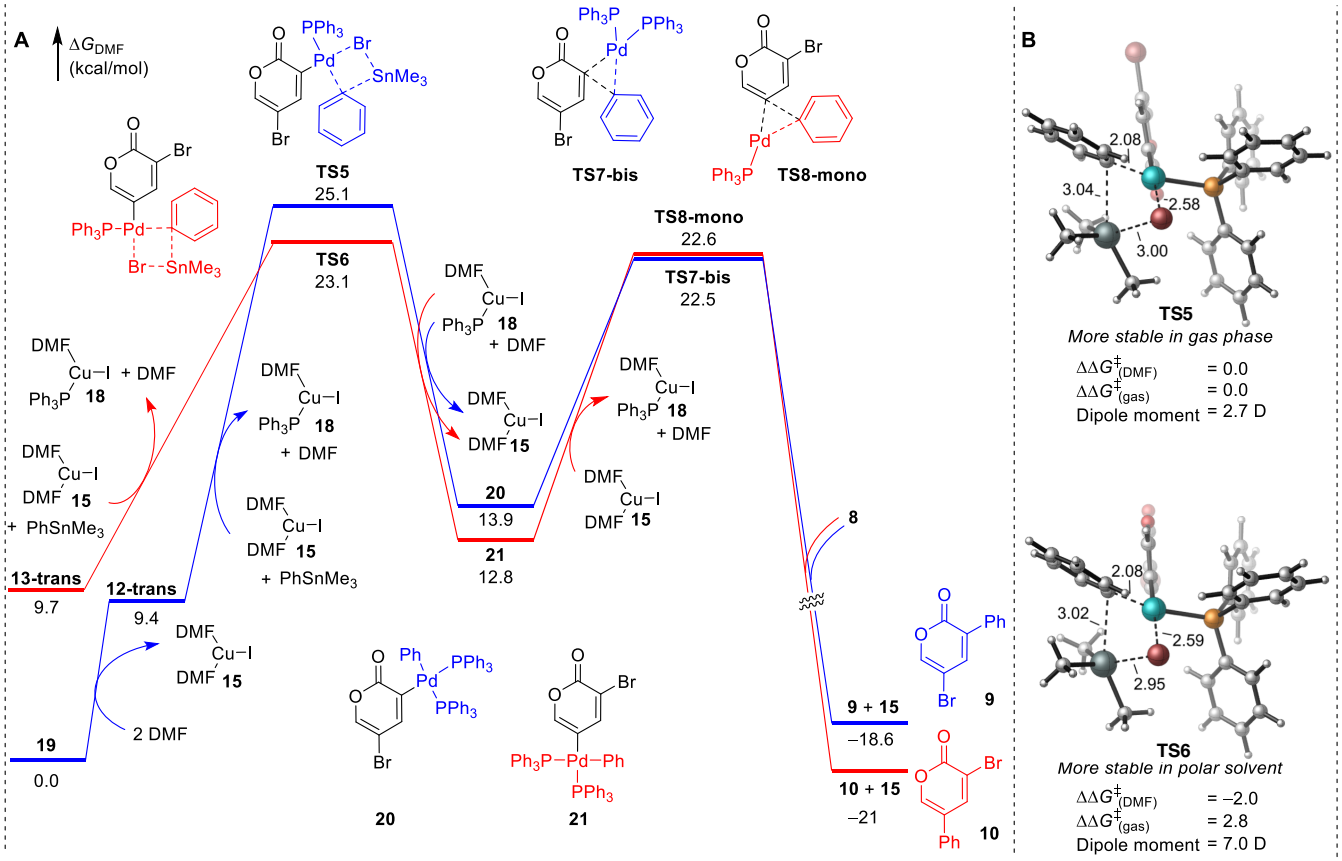

Figure 4. A) Transmetallation and reductive elimination steps in the Pd-catalyzed Stille cross-coupling reaction of 3,5-dibromo-2-pyrone. The C3- and C5-selective pathways are shown in blue and in red, respectively. **B)** Relative activation energies of transmetallation in an implicit solvent ($\Delta\Delta G^{\ddagger}_{DMF}$) and in the gas phase ($\Delta\Delta G^{\ddagger}_{gas}$). All energies in Figure 4A are with respect to **19**, two DMF molecules, and $PhSnMe_3$. The energies in Figure 4B are with respect to **TS5**.

Summary of cross-coupling studies

Scheme 3a provides an overview of our observations regarding the site-selective cross-coupling in 3,5-dibromopyrone. In summary, cross-coupling of **8** gave rise to the C3-coupled product (**9**) as the major product in non-polar solvents (with or without CuI) and in polar solvents in the absence of CuI. The formation of C5-coupled product **10** was favored by conducting the reaction in polar solvents in the presence of CuI. Under these conditions, it was determined that C5 Pd complex **13-cis** is kinetically favored and gives rise to C5-coupled product **10** following a relatively low barrier for transmetallation.

This latter selectivity was computationally established to arise from an initial CuI-assisted PPh_3 dissociation from bis-phosphine ligated Pd complex **14** to give mono-phosphine ligated Pd complex **16** or **17** (Scheme 3b), which has a lower activation barrier to furnish the C5 Pd complex **13-cis**. In addition, when the coupling is conducted in polar solvents in the presence of CuI, the isomeric Pd complexes were found to interconvert. The C3 Pd complex **19** was established to be the thermodynamic oxidative adduct and possesses a higher transmetallation barrier compared to its C5 analog **13-cis**.

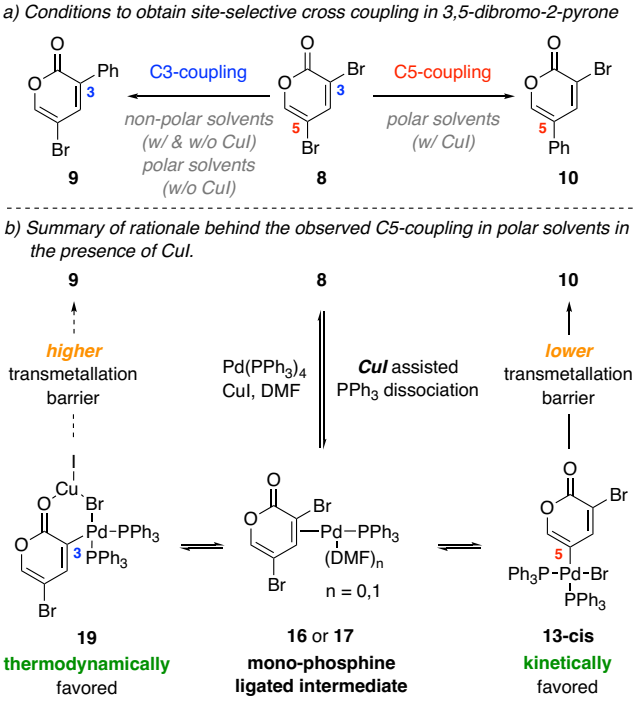

Scheme 3. Summary of experimental/computational results that rationalizes the observed site-selectivity in 3,5-dibromo-2-pyrone

Total Synthesis of delavatine A

Our enhanced mechanistic understanding of the site-selective cross-coupling of 3,5-dibromo-2-pyrone (**8**) positioned us well to complete a synthesis of delavatine A (Scheme 4). In a first step, known vinyl triflate[32] **22** was subjected to Miyaura borylation[33] to furnish vinyl boronate ester **23** in high yield. Next, the conditions initially established by Cho et al. for the site-selective Suzuki coupling of **8** efficiently yielded C5 *mono*-coupled pyrone **26** in 70–75% yield on a 5 g scale. Alternatively, a site-selective Stille coupling of **8** and stannane ester[34] **24** gave **26** in comparable yield. Stille coupling of **26** with known stannane aldehyde[4a] **25** then delivered pseudosymmetric pyrone **27**.

With *bis*-coupled pyrone **27** in hand, we initially sought to open the lactone moiety with an alkoxide in order to induce the desired cascade sequence (cf. **7** → **5**, Scheme 1b). However, under a variety of reaction conditions, the pyrone opening was not successful and resulted merely in decomposition of **27**. Eventually we discovered that pyrone **27** could be cleanly opened in a 1,6-fashion using sodium cyanide,[35] and the resulting carboxylate was alkylated to furnish methyl ester **28**. Impressively, sequential Stille coupling of **8**, **24**, and **25**, followed by pyrone opening could also be achieved to furnish methyl ester **28** directly from **8** in a single pot and in comparable overall yield. A number of conditions were next investigated to convert **28** into a suitable dienolate-like species (cf. **5**, Scheme 1). While deprotonation of the γ-hydrogen of enal **28** using strong bases was unsuccessful, softer enolization conditions cleanly converted **28** to silyl enol ether **29**, providing a precursor for the envisioned 6π-electrocyclization. The major olefin diastereomer in **29** was established as the *E* isomer. We then began exploring conditions for the 6π-electrocyclization and were delighted to find that the desired transformation occurred at elevated temperature in the presence of 1,8-diazabicyclo(5.4.0)undec-7-ene (DBU) to furnish the desired cyclized product (**30**). The entire sequence (silyl enol ether formation, *E*/*Z* isomerization, 6π-electrocyclization, desilylation, and aromatization) can be carried out in a single pot to directly deliver **30** in 25–35% overall yield.[36] Tricycle **30** was then reduced using lithium aluminum hydride, and the corresponding triol was subjected to global Swern oxidation to provide the proposed biosynthetic intermediate **4**. Finally, treatment of trisaldehyde **4** with ammonium acetate led to formation of the isoquinoline moiety to provide delavatine A (**1**), which possessed analytical data (^{1}H and ^{13}C NMR, HRMS, IR, $[\alpha]_D$) in full agreement with those reported for the naturally occurring material.

Scheme 4. Total synthesis of delavatine A

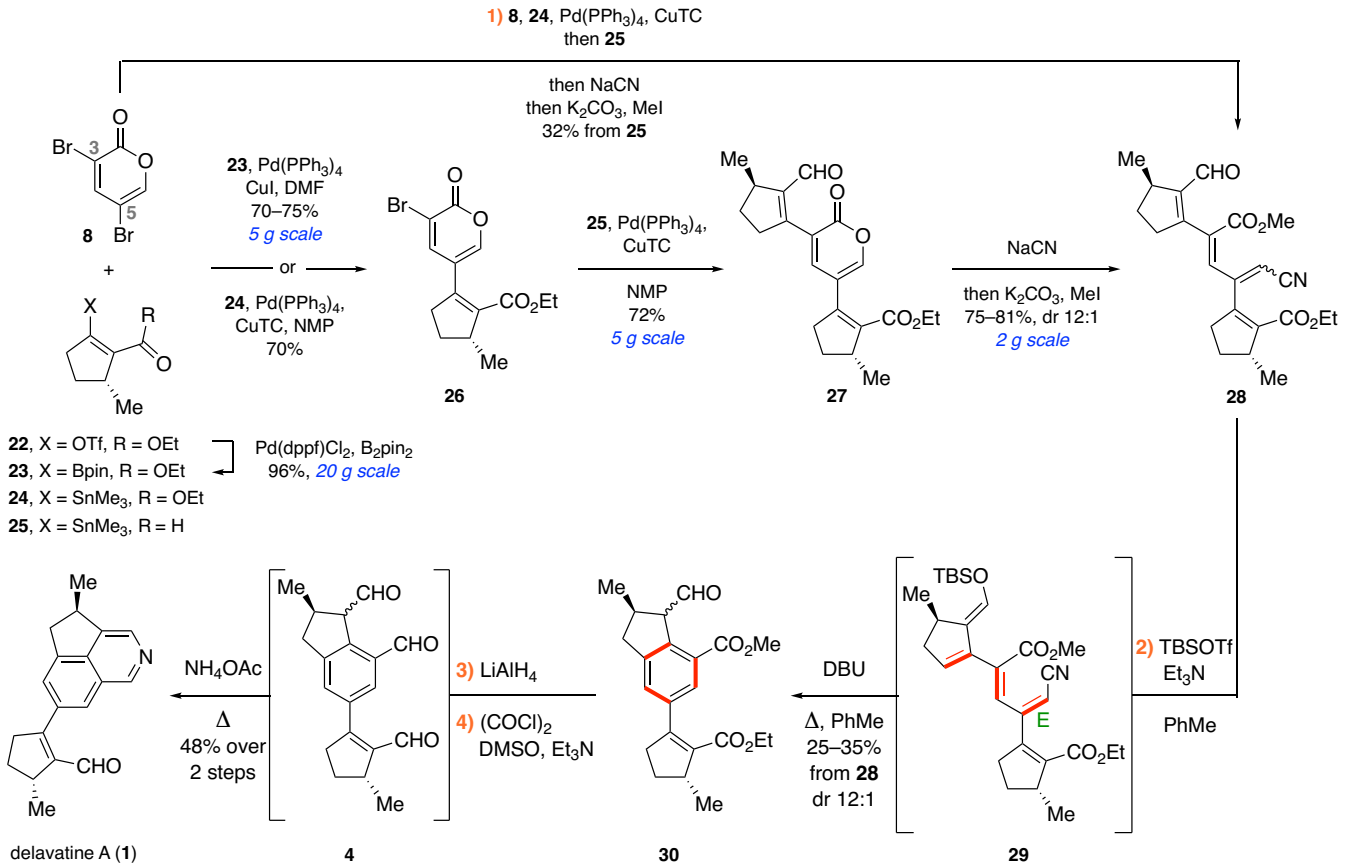

Conclusion

In summary, we have employed computational analysis as a powerful tool to gain insight into the observed site-selective cross-coupling in 3,5-dibromo-2-pyrone. The calculations show that bis-phosphine ligated palladium complexes promote oxidative addition at C3 of 3,5-dibromopyrone as a result of more favorable FMO interactions between the HOMO (d_{xy}) of the Pd complex and the pyrone LUMO (π*). Additionally, combined experimental and computational investigations suggest that the oxidative addition in the presence of CuI proceeds via a pathway that involves a mono-phosphine ligated Pd complex. In this case, the site-selectivity for oxidative addition is diminished and the C5 cross-coupling is preferred due to a more facile transmetallation step. This outcome is attributed to more favorable solvation effects that stabilize the more polar transition state in the C5-selective pathway. These insights may prove valuable in developing a more general understanding of the effects of solvents and CuI additives in site-selective cross couplings in other polyhalogentated heterocycles. The site-selective cross-coupling has enabled a short total synthesis of delavatine A that takes advantage of a strategy inspired by the inherent symmetry of this natural product. The synthesis of **1** proceeds in only four steps from known 3,5-dibromo-2-pyrone **8** (or in a longest linear sequence of ten steps from commercially available (*R*)-pulegone) and features a cascade sequence involving five transformations occurring in a single pot. Our concise and modular route to delavatine A sets the stage for the synthesis of a library of structurally related analogues to facilitate biological studies.

ASSOCIATED CONTENT

Supporting Information

The Supporting Information is available free of charge on the ACS Publications website at http://pubs.acs.org

Experimental details and spectroscopic data (PDF)
Crystallographic data for **12-trans** (CIF)
Crystallographic data for **13-trans** (CIF)

Accession Codes

CCDC 1882829 and 1882830 contain the supplementary crystallographic data for this paper. These data can be obtained free of charge via www.ccdc.cam.ac.uk/data_request/cif, or by emailing data_request@ccdc.cam.ac.uk, or by contacting The Cambridge Crystallographic Data Centre, 12 Union Road, Cambridge CB2 1EZ, UK; fax: +44 1223 336033.

AUTHOR INFORMATION

Corresponding Author

*rsarpong@berkeley.edu
*pengliu@pitt.edu

Notes

The authors declare no competing financial interests.

ACKNOWLEDGMENT

Financial support for this research was provided to R.S. by an ACS PRF New Directions Grant (ACS PRF ND 56509) and to P.L. by the NSF (CHE-1654122). Calculations were performed at the Center for Research Computing at the University of Pittsburgh and the Extreme Science and Engineering Discovery Environment (XSEDE) supported by the NSF. V.P. acknowledges TRDRP for a predoctoral fellowship. C.L.H is grateful for a postdoctoral scholarship from the Swiss National Science Foundation. We thank Prof. C.-G. Cho (Hanyang University, Korea) for insightful discussions regarding studies of the selective cross-coupling chemistry.

REFERENCES

(1) (a) Nakamura, M.; Chi, Y. M.; Yan, W. M.; Nakasugi, Y.; Yoshizawa, T.; Irino, N.; Hashimoto, F.; Kinjo, J.; Nohara, T.; Sakurada, S. Strong antinociceptive effect of incarvillateine, a novel monoterpene alkaloid from *Incarvillea sinensis*. *J. Nat. Prod.* **1999**, *62*, 1293. (b) Nakamura, M.; Kido, K.; Kinjo, J.; Nohara, T. Antinociceptive substances from *Incarvillea delavayi*. *Phytochemistry*, **2000**, *53*, 253. (c) Nakamura, M.; Kido, K.; Kinjo, J.; Nohara, T. Two novel actinidine-type monoterpene alkaloids from *Incarvillea delavayi*. *Chem. Pharm. Bull.* **2000**, *48*, 1826. (d) Nakamura, M.; Chi, Y. M.; Yan, W. M.; Yonezawa, A.; Nakasugi, Y.; Yoshizawa, T.; Hashimoto, F.; Kinjo, J.; Nohara, T.; Sakurada, S. Structure-antinociceptive activity studies of incarvillateine, a monoterpene alkaloid from *Incarvillea sinensis*. *Planta Med.* **2001**, *67*, 114.

(2) (a) Editorial Committee, *Chinese Herb*, Shanghai Science and Technology Publisher, Shanghai, **1999**, *21*, 6435. (b) Chen, Y. Q.; Zhang, W. D.; Kong, L. Y.; Lu, T.; Shen, Y. H. Delavayol, a novel sesquiterpene from *Incarvillea delavayi* Bureau et Franchet. *Nat. Prod. Res.* **2010**, *24*, 915.

(3) Zhang, Z.; Yang, F.; Fu, J.-J.; Shen, Y.-H.; He, W.; Zhang, W.-D. Delavatine A, a structurally unusual cyclopenta[*de*]isoquinoline alkaloid from *Incarvillea delavayi*. *RSC Adv.* **2016**, *6*, 65885.

(4) (a) Zhang, Z.; Wang, J.; Li, J.; Yang, F.; Liu, G.; Tang, W.; He, W.; Fu, J.-J.; Shen, Y.-H.; Li, A.; Zhang, W.-D. Total synthesis and stereochemical assignment of delavatine A: Rh-catalyzed asymmetric hydrogenation of indene-type tetrasubstituted olefins and kinetic resolution through Pd-catalyzed triflamide-directed C–H olefination. *J. Am. Chem. Soc.* **2017**, *139*, 5558. (b) Recently also a formal synthesis of delavatine A was reported, Peez, T.; Luy, J.-N.; Harms, K. Tonner, R.; Koert, U. From acenaphthenes to (+)-delavatine A: Visible-light-induced ring closure of methyl (α-naphthyl) acrylates. *Chem. Eur. J.* **2018**, *24*, 17686.

(5) For selected total syntheses leveraging symmetry, see: (a) Aube, J.; Ghosh, S.; Tanol, M. Symmetry-driven synthesis of indole alkaloids: asymmetric total syntheses of (+)-yohimbine, (-)-yohimbone, (-)-yohimbane, and (+)-alloyohimbane. *J. Am. Chem. Soc.* **1994**, *116*, 9009. (b) Ball, M.; Gaunt, M. J.; Hook, D. F.; Jessiman, A. S.; Kawahara, S.; Orsini, P.; Scolaro, A.; Talbot, A. C.; Tanner, H. R.; Yamanoi, S.; Ley, S. V. Total synthesis of spongistatin 1: A synthetic strategy exploiting its latent pseudo-symmetry. *Angew. Chem. Int. Ed.* **2005**, *44*, 5433. (c) Mahapatra, S.; Carter, R. G. Exploiting hidden symmetry in natural products: Total syntheses of amphidinolides C and F. *J. Am. Chem. Soc.* **2013**, *135*, 10792. (d) Kisunzu, J. K.; Sarpong, R. Hidden symmetry enables a 15-step total synthesis of pactamycin. *Angew. Chem. Int. Ed.* **2013**, *52*, 10694. (e) Ellerbrock, P.; Armanino, N.; Trauner, D. Biomimetic synthesis of the calcineurin phosphatase inhibitor dibefurin. *Angew. Chem. Int. Ed.* **2014**, *53*, 13414. (f) Wang,

T.; Hoye, T. R. Diels–Alderase-free, bis-pericyclic, [4+2] dimerization in the biosynthesis of (±)-paracaseolide A. *Nat. Chem.* **2015**, *7*, 641. (g) Ellerbrock, P.; Armanino, N.; Ilg, M. K.; Webster, R.; Trauner, D. An eight-step synthesis of epicolactone reveals its biosynthetic origin. *Nat. Chem.* **2015**, *7*, 879. (h) Park, J.; Chen, D. Y.-K. A desymmetrization-based total synthesis of reserpine. *Angew. Chem. Int. Ed.* **2018**, *57*, 16152.

(6) For selected total syntheses involving 6π electrocyclization/aromatization, see: (a) Abe, T.; Ikeda, T.; Yanada, R.; Ishikura, M. Concise total synthesis of calothrixins A and B. *Org. Lett.* **2011**, *13*, 3356. (b) Lu, Z.; Li, Y.; Deng, J.; Li, A. Total synthesis of the daphniphyllum alkaloid daphenylline. *Nat. Chem.* **2013**, *5*, 679. (c) Li, J.; Yang, P.; Yao, M.; Deng, J.; Li, A. Total synthesis of rubriflordilactone A. *J. Am. Chem. Soc.* **2014**, *136*, 16477. (d) Yang, M.; Li, J.; Li, A. Total synthesis of clostrubin. *Nat. Commun.* **2015**, *6*, 6445. (e) Yamaguchi, A. D.; Chepiga, K. M.; Yamaguchi, J.; Itami, K.; Davies, H. M. L. Concise syntheses of dictyodendrins A and F by a sequential C−H functionalization strategy. *J. Am. Chem. Soc.* **2015**, *137*, 644. (f) Meng, Z.; Haixin, Yu.; Li, L.; Tao, W.; Chen, H.; Wan, M.; Yang, P.; Edmonds, D. J.; Zhong, J.; Li, A. Total synthesis and antiviral activity of indolosesquiterpenoids from the xiamycin and oridamycin families. *Nat. Commun.* **2015**, *6*, 6096. (g) Yang, P.; Yao, M.; Li, J.; Li, Y.; Li, A. Total synthesis of rubriflordilactone B. *Angew. Chem. Int. Ed.* **2016**, *55*, 6964. (h) Yang, M.; Yang, X.; Sun, H.; Li, A. Total synthesis of ileabethoxazole, pseudopteroxazole, and *seco*-pseudopteroxazole. *Angew. Chem. Int. Ed.* **2016**, *55*, 2851. (i) Li, H.; Chen, Q.; Lu, Z.; Li, A. Total syntheses of aflavazole and 14-hydroxyaflavinine. *J. Am. Chem. Soc.* **2016**, *138*, 15555.

(7) Cho, H. K.; Nishii, A.; Cho, C.-G. Preparation of 3,5-dibromo-2-pyrone from coumalic acid. *Org. Synth.* **2015**, *92*, 148.

(8) Fairlamb, I. J. S. Regioselective (site-selective) functionalisation of unsaturated halogenated nitrogen, oxygen and sulfur heterocycles by Pd-catalysed cross-couplings and direct arylation processes. *Chem. Soc. Rev.* **2007**, *36*, 1036 and references therein.

(9) For site-selective Sonogashira coupling of 3,5-dibromo-2-pyrone see, Lee, J.-H.; Park, J.-S.; Cho, C.-G. Regioselective synthesis of 3-alkynyl-5-bromo-2-pyrones via Pd-catalyzed couplings on 3,5-dibromo-2-pyrone. *Org. Lett.* **2002**, *4*, 1171.

(10) For site-selective Stille coupling of 3,5-dibromo-2-pyrone see, Kim, W.-S.; Kim, H.-J.; Cho, C.-G. Regioselectivity in the Stille coupling reactions of 3,5-dibromo-2-pyrone. *J. Am. Chem. Soc.* **2003**, *125*, 14288.

(11) For site-selective Suzuki coupling of 3,5-dibromo-2-pyrone see, Ryu, K.-M.; Gupta, A. K.; Han, J. W.; Oh, C. H.; Cho, C.-G. Regiocontrolled Suzuki-Miyaura couplings of 3,5-dibromo-2-pyrone. *Synlett* **2004**, *12*, 2197.

(12) For recent studies on site-selective cross coupling of polyhalogenated heterocycles, see: (a) Schröter, S.; Stock, C.; Bach, T. Regioselective cross-coupling reactions of multiple halogenated nitrogen-, oxygen-, and sulfur-containing heterocycles. *Tetrahedron* **2005**, *61*, 2245. (b) Golding, W. A. Higgins, R. P.; Phipps, R. J. Site-selective cross-coupling of remote chlorides enabled by electrostatically directed palladium catalysis. *J. Am. Chem. Soc.* **2018**, *140*, 13570. (c) Keylor, M. H.; Niemeyer, Z. L.; Sigman, M. S.; Tan, K. L. Inverting conventional chemoselectivity in Pd-catalyzed amine arylations with multiply halogenated pyridines. *J. Am. Chem. Soc.* **2017**, *139*, 10613. (d) Strotman, N. A.; Chobanian, H. R.; He, J.; Guo, Y.; Dormer, P. G.; Jones, C. M.; Steves, J. E. Catalyst-controlled regioselective Suzuki couplings at both positions of dihaloimidazoles, dihalooxazoles, and dihalothiazoles. *J. Org. Chem.* **2010**, *75*, 1733. (e) Dai, X.; Chen, Y.; Garrell, S.; Liu, H.; Zhang, L.-K.; Palani, A.; Hughes, G.; Nargund, R. Ligand-dependent site-selective Suzuki cross-coupling of 3,5-dichloropyridazines. *J. Org. Chem.* **2013**, *78*, 7758.

(13) (a) Zhang, H.; Cravillion, T.; Lin, N.-K.; Tian, Q.; Beaudry, D.; Defreese, J. L.; Fettes, A.; James, P.; Linder, D.; Malhotra, S.; Han, C.; Angelaud, R.; Gosselin, F. Development of an efficient manufacturing process for reversible Bruton's tyrosine kinase inhibitor GDC-0853. *Org. Process Res. Dev.* **2018**, *22*, 978. (b) Tam, N. T.; Jung, E.-J.; Cho, C.-G. Intramolecular imino Diels–Alder approach to the synthesis of the aspidosperma alkaloid from 3,5-dibromo-2-pyrone. *Org. Lett.* **2010**, *12*, 2012. (c) Chang, J. H.; Kang, H.-U.; Jung, I.-H.; Cho, C.-G. Total synthesis of (±)-galanthamine via a C3-selective Stille coupling and IMDA cycloaddition cascade of 3,5-dibromo-2-pyrone. *Org. Lett.* **2010**, *12*, 2016. (d) Tam, N. T.; Cho, C.-G. Total synthesis of (±)-crinine via the regioselective Stille coupling and Diels–Alder reaction of 3,5-dibromo-2-pyrone. *Org. Lett.* **2008**, *10*, 601. (e) Lee, J.-H.; Cho, C.-G. H-bonding mediated asymmetric intramolecular Diels–Alder reaction in the formal synthesis of (+)-aplykurodinone-1. *Org. Lett.* **2018**, *20*, 7312.

(14) (a) Legault, C. Y.; Garcia, Y.; Merlic, C. A. Houk, K. N. Origin of regioselectivity in palladium-catalyzed cross-coupling reactions of polyhalogenated heterocycles. *J. Am. Chem. Soc.* **2007**, *129*, 12664. (b) Garcia, Y.; Schoenebeck, F.; Legault, C. Y.; Merlic, C. A. Houk, K. N. Theoretical bond dissociation energies of halo-heterocycles: Trends and relationships to regioselectivity in palladium-catalyzed cross-coupling reactions. *J. Am. Chem. Soc.* **2009**, *131*, 6632.

(15) Handy, S. T.; Zhang, Y. A simple guide for predicting regioselectivity in the coupling of polyhaloheteroaromatics. *Chem. Commun.* **2006**, 299.

(16) In our hands, cross-coupling did not proceed at room temperature in the absence of CuI in any of the investigated solvents.

(17) Interestingly and in contrast to Ref. 10, when the oxidative addition was carried out with a stoichiometric amount of $Pd(PPh_3)_4$, formation of C5-Pd complex **13** was not observed and only C3-Pd complex **12** could be isolated. See the Supporting Information for experimental details.

(18) a) Vogel, A. I.; Furniss, B. S.; Hannaford, A. J.; Smith, P. W. G.; Tatchell, A. R. Vogel's Textbook of practical organic chemistry (5th Edition); Pearson Education Limited: Essex, 1989. b) https://www.organicdivision.org/orig/organic_solvents.html (Retrieved October, 2018).

(19) The X-ray structures of **12** and **13** were also reported in ref. 10.

(20) See the Supporting Information for further details.

(21) Seeman, J. Effect of conformational change on reactivity in organic chemistry. Evaluations, applications, and extensions of Curtin-Hammett Winstein-Holness kinetics. *Chem. Rev.* **1983**, *83*, 83 and references therein.

(22) Jones, G. O.; Liu, P.; Houk, K. N.; Buchwald, S. L. Computational explorations of mechanisms and ligand-directed selectivities of copper-catalyzed Ullmann-type reactions. *J. Am. Chem. Soc.* **2010**, *132*, 6205. (b) Yu, H-Z.; Jiang, Y-Y.; Fu, Y.; Liu, L. Alternative mechanistic explanation for ligand-dependent selectivities in copper-catalyzed *N*- and *O*-arylation reactions. *J. Am. Chem. Soc.* **2010**, *132*, 18078.

(23) (a) McMullin, C. L.; Fey, N.; Harvey, J. N. Computed ligand effects on the oxidative addition of phenyl halides to phosphine supported palladium(0) catalysts. *Dalton Trans.* **2014**, *43*, 13545. (b) Kozuch, S.; Martin, J. M. L. What makes for a bad catalytic cycle? A theoretical study on the Suzuki–Miyaura reaction within the energetic span model. *ACS Catal.* **2011**, *1*, 246.

(24) (a) Farina, V.; Kapadia, S.; Krishnan, B.; Wang, C.; Liebeskind, L. S. On the nature of the "copper effect" in the Stille cross-coupling. *J. Org. Chem*. **1994**, *59*, 5905. (b) Beaupérin, M.; Job, A.; Cattey, H.; Royer, S.; Meunier, P.; Hierso, J.-C. Copper(I) iodide polyphosphine adducts at low loading for Sonogashira alkynylation of demanding halide substrates: Ligand exchange study between copper and palladium. *Organometallics* **2010**, *29*, 2815. (c) Aufiero, M.; Proutiere, F.; Schoenebeck, F. Redox reactions in palladium catalysis: On the accelerating and/or inhibiting effects of copper and silver salt additives in cross-coupling chemistry involving electron-rich phosphine ligands. *Angew. Chem. Int. Ed.* **2012**, *51*, 7226.

(25) (a) Li, Z.; Fu, Y.; Guo, Q.-X.; Liu, L. Theoretical study on monoligated Pd-catalyzed cross-coupling reactions of aryl chlorides and bromides. *Organometallics* **2008**, *27*, 4043. (b) Lam, K. C.; Marder, T. B.; Lin, Z. DFT studies on the effect of the nature of the aryl halide Y–C_6H_4–X on the mechanism of its oxidative addition to Pd^0L versus Pd^0L_2. *Organometallics* **2007**, *26*, 758. (c) Ahlquist, M.; Norrby, P.-O. Oxidative addition of aryl chlorides to monoligated palladium(0): A DFT-SCRF study. *Organometallics* **2007**, *26*, 550.

(26) The ligand exchange energies to form **16** and **15** were calculated with respect to **14** and a three-coordinated $(DMF)_2CuI$ complex as the energy zero. We cannot rule out the formation of CuI oligomers under the reaction conditions. However, the polar solvent (DMF) is expected to promote the formation of the CuI monomer.

(27) (a) Bickelhaupt, F. M.; Houk, K. N. Analyzing reaction rates with the distortion/interaction-activation strain model. *Angew. Chem. Int. Ed.* **2017**, *56*, 10070. (b) Ess, D. H.; Houk, K. N. Distortion/interaction energy control of 1,3-dipolar cycloaddition reactivity. *J. Am. Chem. Soc.* **2007**, *129*, 10646.

(28) The effects of bond dissociation energy and steric environment on regioselectivity were also considered. See the Supporting Information for detailed discussions.

(29) Schoenebeck, F.; Houk, K. N. Ligand-controlled regioselectivity in palladium-catalyzed cross coupling reactions. *J. Am. Chem. Soc.* **2010**, *132*, 2496.

(30) Unfortunately, to date, we have not been able to computationally locate energy values that support the experimentally observed Curtin-Hammett scenario. The exact mechanism for the reversible oxidative addition remains unclear.

(31) (a) Álvarez, R.; Faza, O. N.; de Lera, A. R.; Cardenas, D. J. A density functional theory study of the Stille cross-coupling *via* associative transmetalation. The role of ligands and coordinating solvents. *Adv. Synth. Catal.* **2007**, *349*, 887. (b) Ren, Y.; Jia, J.; Liu, W.; Wu, H.-S. Theoretical study on the mechanism of palladium-catalyzed dearomatization reaction of chloromethylnaphthalene. *Organometallics* **2013,** *32*, 52. (c) Álvarez, R.; Faza, O. N.; López, C. S.; de Lera, Á. R. Computational characterization of a complete palladium-catalyzed cross-coupling process: The associative transmetalation in the Stille reaction. *Org. Lett.* **2006,** *8*, 35. (d) Álvarez, R.; Pérez, M.; Faza, O. N.; de Lera, A. R. Associative transmetalation in the Stille cross-coupling reaction to form dienes : Theoretical insights into the open pathway. *Organometallics* **2008,** *27*, 3378. (e) Carrizo, E. D. S.; Fernández, I.; Martin, S. E. Computational study on the C–heteroatom bond formation via Stille cross-coupling reaction: Differences between organoheterostannanes $Me_3SnAsPh_2$ vs Me_3SnPPh_2. *Organometallics* **2015,** *34*, 159. (f) Nova, A.; Ujaque, G.; Maseras, F.; Lledós, A.; Espinet, P. A critical analysis of the cyclic and open alternatives of the transmetalation step in the Stille cross-coupling reaction. *J. Am. Chem. Soc.* **2006,** *128*, 14571.

(32) Hugelshofer, C. L.; Magauer, T. A general entry to antifeedant sesterterpenoids: Total synthesis of (+)-norleucosceptroid A, (–)-norleucosceptroid B, and (–)-leucosceptroid K. *Angew. Chem. Int. Ed.* **2014**, *53*, 11351.

(33) (a) Miyaura, N.; Yamada, K.; Suzuki, A. A new stereospecific cross-coupling by the palladium-catalyzed reaction of 1-alkenylboranes with 1-alkenyl or 1-alkynyl halides. *Tetrahedron Lett.* **1979**, *20*, 3437. (b) Miyaura, N.; Suzuki, A. Stereoselective synthesis of arylated (*E*)-alkenes by the reaction of alk-1-enylboranes with aryl halides in the presence of palladium catalyst. *J. Chem. Soc., Chem. Commun.* **1979**, 866.

(34) The methyl ester derivative of **13** is known, see Ref. 4.

(35) For reactions of pyrone with cyanide ion, see: (a) Blumberg, L. C.; Costa, B.; Goldstein, R. Chemoselective 1,3-dipolar cycloadditions of azomethine ylide with conjugated dienes. *Tetrahedron Lett.* **2011**, *52*, 872. (b) Vogel, G. Reaction of 2-pyrones with cyanide Ion. *J. Org. Chem.* **1965**, *30*, 203.

(36) A summary of the reaction conditions investigated for this cascade sequence is included in the SI.

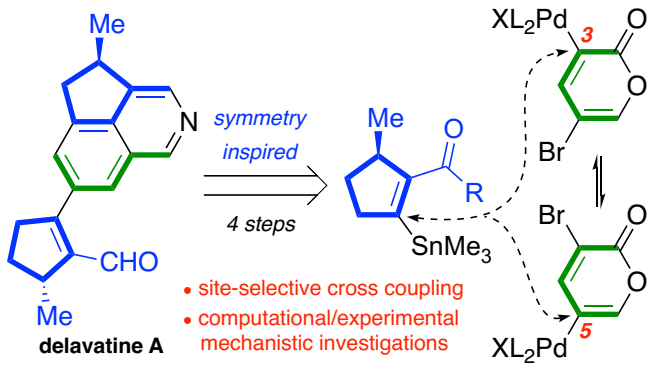
Me
N
CHO
Me
delavatine A
symmetry
inspired
4 steps
Me
O
R
SnMe3
XL2Pd
3
O
O
Br
Br
O
O
5
XL2Pd
• site-selective cross coupling
• computational/experimental
mechanistic investigations